Hindawi
Advances in Condensed Matter Physics
Volume 2020, Article ID 8850701, 11 pages
https://doi.org/10.1155/2020/8850701

Research Article

Tuning Structural, Electronic, and Magnetic Properties of C Sites Vacancy Defects in Graphene/MoS_2 van der Waals Heterostructure Materials: A First-Principles Study

Hari Krishna Neupane [1,2] **and Narayan Prasad Adhikari** [2]

[1]*Amrit Campus, Institute of Science and Technology Tribhuvan University, Kathmandu, Nepal*
[2]*Central Department of Physics, Institute of Science and Technology Tribhuvan University, Kathmandu, Nepal*

Correspondence should be addressed to Narayan Prasad Adhikari; npadhikari@gmail.com

Received 28 August 2020; Revised 31 October 2020; Accepted 17 November 2020; Published 29 November 2020

Academic Editor: Da-Ren Hang

In this work, we systematically studied the structure, and electronic and magnetic properties of van der Waals (vdWs) interface Graphene/MoS_2 heterostructure (HS-G/MoS_2) and C sites vacancy defects in HS-G/MoS_2 materials using first-principles calculations. By the structural analysis, we found that nondefects geometry is more compact than defects geometries. To investigate the electronic and magnetic properties of HS-G/MoS_2 and C sites vacancy defects in HS-G/MoS_2 materials, we have studied band structure, density of states (DOS), and partial density of states (PDOS). By analyzing the results, we found that HS-G/MoS_2 is metallic in nature but C sites vacancy defects in HS-G/MoS_2 materials have a certain energy bandgap. Also, from the band structure calculations, we found that Fermi energy level shifted towards the conduction band in vacancy defects geometries which reveals that the defected heterostructure is n-type Schottky contacts. From DOS and PDOS analysis, we obtained that the nonmagnetic HS-G/MoS_2 material changes to magnetic materials due to the presence of C sites vacancy defects. Right 1C atom vacancy defects (R-1C), left 1C atom vacancy defects (L-1C), centre 1C atom vacancy defects (C-1C), and 2C (1C right and 1C centre) atom vacancy defects in HS-G/MoS_2 materials have magnetic moments of −0.75 μ_B/cell, −0.75 μ_B/cell, −0.12 μ_B/cell, and +0.39 μ_B/cell, respectively. Electrons from 2s and 2p orbitals of C atoms have main contributions for the magnetism in all these materials.

1. Introduction

Graphene has a honeycomb lattice of carbon atoms; each atom in a lattice contains four valence electrons and interacts with its three nearest neighbor carbon through σ-bond due to sp^2 hybridization of 2s, $2p_x$, and $2p_y$ orbitals of three valence electrons. The fourth electron occupies the $2p_z$ orbital which overlaps with the nearest $2p_z$ electrons and forms a π-bond perpendicular to the Graphene plane. These electrons are loosely bound, and most of the electronic properties of the pure Graphene are dictated by these delocalized electrons [1, 2]. The band structure of the pure Graphene (two bands π and π^*) originating from p_z-orbital meets at six points in k-space known as Dirac points. Dirac points of Graphene are formed at the Fermi energy level, so it is called zero bandgap semiconductors. The structure of Graphene containing Dirac points bears astonishing electronic, optical, mechanical, and magnetic properties, so electronic devices, transparent electrodes, and spintronics devices can be manufactured by using Graphene [1–3]. In nanoscience research, a keen interest is given by the researchers for the study of two-dimensional hexagonal structural materials. Like Graphene, MoS_2 monolayer is a 2D transition metal dichalcogenide (TMDC) honeycomb structure material with a direct bandgap of the value of 1.80 eV [4]. It also has winsome properties, because of which it can be applied in industry for producing signal amplifier, integrated logic circuits, flexible optoelectronic devices, transistors, photodetectors, photocatalysts, optoelectronic devices, solar cells, and lubricants. Fundamentally, also it is

interesting as it is just a single-layered material [5–10]. The Graphene-based research in 2D materials has made enormous success [11–13]. The metal/semiconductor interface such as G/MoS_2 is a new contact type of the Graphene-based van der Waals (vdWs) interface, known as heterostructures (HS) material. The heterostructures can be used to wipe out the unwanted properties of the constituents and hence give rise to desired properties than the constituents [14]. The first-principles study of HS-G/MoS_2 can be done in periodically repeated supercells. The supercells contain two interfaces which are equivalent to the term of stoichiometry and geometry [15]. This G/MoS_2 vdWs interface was studied by various research groups [15, 16]. The report presented that the structure contains some innovative properties which can create different components in the electronic devices [17]. Also, vdWs HS-G/MoS_2 has intriguing electronic properties, transport properties, optical transparency, mechanical flexibility, and photoconductivity. Thus, it can be highly recommended in the application of electronic, photovoltaic, and memory devices [18–21].

In our previous work, we studied structural, electronic, and magnetic properties of Mo sites vacancy defects in HS-G/MoS_2 materials by first-principles calculations using vdWs correction in the DFT-D2 approach [22]. To the best of our knowledge, C sites vacancy defects in HS-G/MoS_2 materials have not been studied. Therefore, in the present work, we investigated the structural, electronic, and magnetic properties of vdWs interfaces, HS-G/MoS_2, and C sites vacancy defects in HS-G/MoS_2 materials using first-principles calculations with the DFT-D2 approach. The vacancy defects in solids cause deviation of atoms or ions from the periodicity, and they are used to find innovative properties. They can be used to design new materials [23]. Also, the magnetic materials can be applied in various fields such as biomedicine, molecular biology, biochemistry, diagnosis, catalysis, nanoelectronic devices, and various other industrial applications like magnetic seals in motors, magnetic sensors, magnetic inks, electrical power generator, transformers, magnetic recording media, and computers [24, 25].

The rest part of the paper is organized as follows. The computational details will be discussed in Section 2 whereas Section 3 contains results and discussion. We close the paper with the main conclusions and outlook of the present work in Section 4.

2. Computational Model and Methods

We have performed the first-principles calculations to investigate the structural, electronic, and magnetic properties of HS-G/MoS_2 and C atom vacancy defects in HS-G/MoS_2 materials within the framework of density functional theory (DFT) [26], with van der Waals (vdWs) corrections taken into account by DFT-D2 [27] approach using Quantum ESPRESSO (QE) computational package [28]. To incorporate the electronic exchange and correlation effects in the density functional theory, Generalized Gradient Approximation (GGA) was used via Perdew-Burke-Ernzerhof (PBE) exchange correlations [29]. Grimme's Rappe-Rabe-Kaxiras-Joannopoulos (RRJK) model of ultrasoft pseudopotentials is used to replace the complicated effects of the motion of the core (i.e., nonvalence) electrons of an atom and its nucleus with an effective potential for all atoms in a system. It helps to deal with only the chemically active valence electrons which are included explicitly in our calculations. The electronic configurations of valence electrons in C, Mo, and S atoms of our system are C:[He] $2s^2 2p^2$, Mo:[Kr] $4d^5 5s^1$, and S:[Ne] $3s^2 3p^4$, respectively. All the structures are optimized and relaxed by the BFGS scheme [30], using Quantum ESPRESSO code [28], until the total energy changes are less than 10^{-4} Ry and force acting between two consecutive self-consistent fields is less than 10^{-3} Ry/Bohr. After the relax calculations, we have done self-consistent total energy calculations, for this Brillouin zone of heterostructure is sampled in k-space using Monkhorst-Pack (MP) scheme [31], with an appropriate number of mesh $(4 \times 4 \times 1)$ of k-points, which is determined from the convergence test. The Marzari-Vanderbilt (MV) [32] smearing of the small width of 0.001 Ry is used. In addition, we have chosen the "David" diagonalization method with a "plain" mixing mode and mixing factor of 0.6 for self-consistency. For band structure calculations, a mesh of $(4 \times 4 \times 1)$ k-points is used, and for the density of states (DOS) and partial density of states (PDOS) calculations, an automatic denser mesh of $(8 \times 8 \times 1)$ k-points is used, where, in both the cases, 100 k-points are chosen along the high symmetric points connecting the reciprocal space.

In this work, we have prepared the HS-G/MoS_2 by using (4×4) supercell structure of Graphene and (3×3) supercell structure of monolayer MoS_2 with lattice mismatch about 4.13%, where we maintained vacuum distance greater than 20 Å to avoid the interactions between two adjacent layers as shown in Figure 1(c). For the construction of these supercell structures, at first, we have created a unit cell of Graphene and MoS_2 by using structural analysis tool XCrySDen and computational tool Quantum ESPRESSO. To construct the unit cell, we used the Bravais lattice index, cell dimension parameters, and lattice constant in the input file. For the Graphene unit cell, we have taken the experimentally reported value of the distance between two carbon atoms that is 1.42 Å [31]. After the construction of the Graphene unit cell, we calculated the kinetic energy cut-off value, k-points, and lattice parameters from the convergence test and found the constant kinetic energy cut-off value 35 Ry. The charge density cut-off value for ultrasoft pseudopotential is calculated by using the relation $10 \times$ kinetic energy cut-off, which is 350 Ry. These obtained parameters (kinetic energy cut-off, charge density cut-off, k-points, and lattice parameters) are used in the input file to relax our system. We found the distance between two carbon atoms of the relaxed Graphene unit cell to be 1.42 Å, which is very close to the starting value for relaxation [31]. The unit cell of MoS_2 is prepared by using the experimental value of 3.19 Å [6, 33]. Its unit cell contains a single layer of two S and one Mo atoms. The Mo atom bounds with the S atom in a trigonal prismatic arrangement, where each Mo atom is surrounded by six first neighboring S atoms. After the construction of a unit cell, we have calculated its optimized values of kinetic energy cut-off, k-points, lattice parameters, and charge

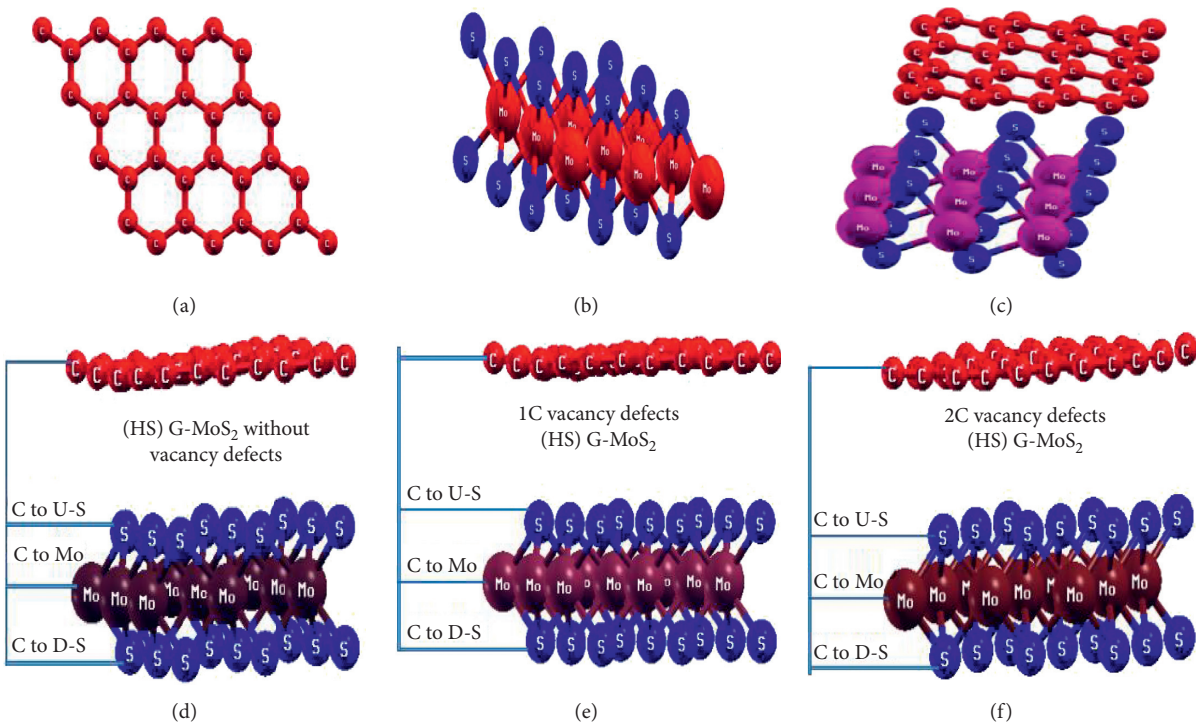

FIGURE 1: (a) (4 × 4) supercell structure of Graphene. (b) (3 × 3) supercell structure of MoS_2. (c) Heterostructure of G/MoS_2. (d) Interlayer and interatomic distances measurement geometry of HS-G/MoS_2. (e) Interlayer and interatomic distances measurement geometry of 1C atom vacancy defects in HS-G/MoS_2. (f) Interlayer and interatomic distances measurement geometry of 2C atom vacancy defects in HS-G/MoS_2.

density cut-off values as in Graphene, and then these parameters are used in the input file to relax the system. We found that the value of the lattice constant to be 3.18 Å, which is also close to the experimentally reported value of 3.19 Å [6, 33]. We then developed (4 × 4) supercell structure of Graphene and (3 × 3) supercell of monolayer MoS_2 from these prepared unit cells, by extending along x and y direction as shown in Figures 1(a) and 1(b), respectively. After that, we have constructed the stable and relaxed structures of right 1C atom vacancy defects (R-1C), left 1C atom vacancy defects (L-1C), centre 1C atom vacancy defects (C-1C), and 2C (1C right and 1C centre) atom vacancy defects in HS-G/MoS_2 as shown in Figure 2. These prepared structures are used for further investigations.

3. Results and Discussion

In the present work, we have carried out a first-principles study of C sites vacancy defects in HS-G/MoS2 heterostructures. In this section, we present the main findings and their interpretations from the investigation of the heterostructures.

3.1. Structural Analysis. The Graphene-based stable heterostructure materials in G/MoS_2 is prepared by using (4 × 4) supercell structure of Graphene and (3 × 3) supercell structure of monolayer MoS_2 with considerable (4.13%) lattice mismatch as shown in Figures 1(a)–1(c). The stability of the structure is determined by binding energy calculations. The higher the value of binding energy is, the more stable the system is. Thus, the greater value of binding energy material is more favorable for the calculations of its physical properties. The binding energy (E_b) of HS-G/MoS_2 is calculated by using the following relation: $E_b = E_{Graphene} + E_{MoS2} - E_{HS\text{-}G/MoS2}$, where $E_{Graphene}$, E_{MoS2}, and $E_{HS\text{-}G/MoS2}$ represent the ground state energy of a fully relaxed (4 × 4) supercell of Graphene, (3 × 3) supercell of MoS_2, and heterostructure of G/MoS_2, respectively. The heterostructures of carbon atom vacancy defects are prepared by using optimized and relaxed HS-G/MoS_2 material as shown in Figure 2, where out of 32C atoms, the concentrations of the vacancy defects of R-1C, L-1C, C-1C, and 2C in HS-G/MoS_2 materials are found to be 3.13%, 3.13%, 3.13%, and 6.25%, respectively. These are also stable structures. The order of binding energy of the structures is found to be as HS-G/MoS_2 > 1C atoms HS-G/MoS_2 > 2C atoms HS-G/MoS_2 as given in Table 1. So, the stability of the structure is decreased with an increase in its defects concentrations. Among the various carbon atom vacancy defects in HS-G/MoS_2 configurations, we have used the most stable R-1C, L-1C, C-1C, and 2C atom vacancy defects in HS-G/MoS_2 materials. R-1C, L-1C, C-1C, and 2C atom vacancy defects in HS-G/MoS_2 have defects formation energies of 0.20 eV, 0.20 eV, 0.20 eV, and 0.41 eV, respectively. These energy values are less than the defects formation of energy values of other vacancy defects configurations. The defects formation energies in our systems are calculated based on the standard formalism [34]; $E_f = E_T(defect) + n_C\mu_C - E_T(perfect)$, where E_T $(defect)$ is the

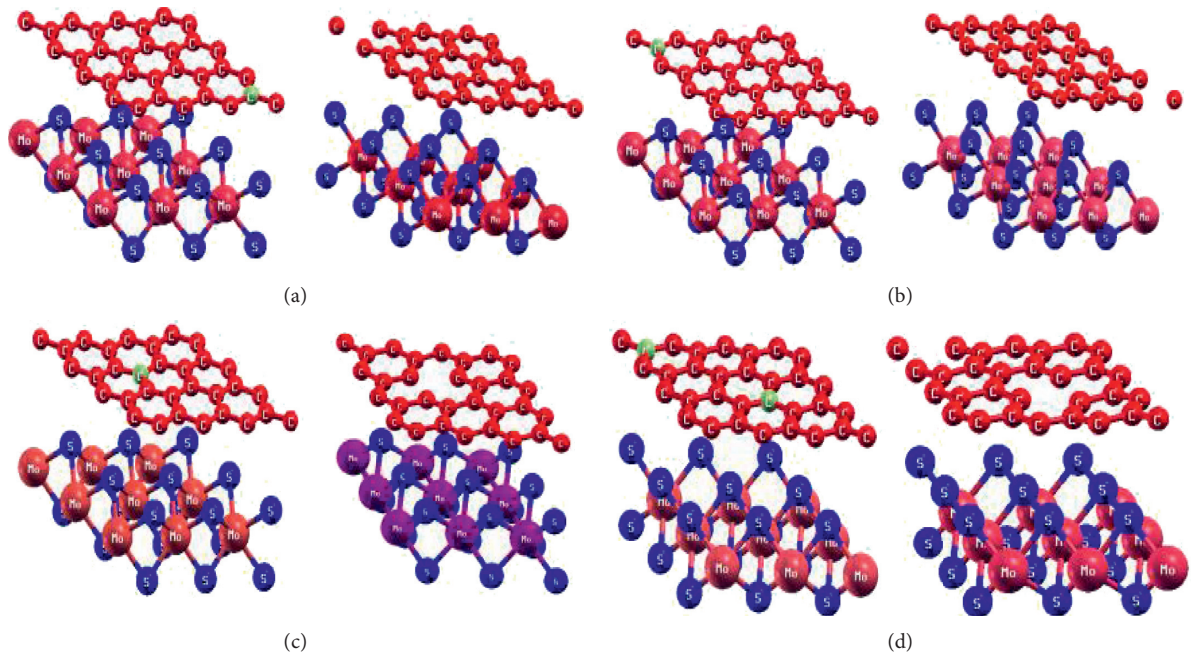

Figure 2: Optimized and relaxed structures of C sites vacancy defects in HS-G/MoS_2 materials. (a) R-1C atom vacancy defects in HS-G/MoS_2. (b) L-1C atom vacancy defects in HS-G/MoS_2. (c) C-1C atom vacancy defects in HS-G/MoS_2. (d) 2C atom vacancy defects in HS-G/MoS_2.

Table 1: Fermi energy level (E_f), Fermi energy level shift towards conduction band (E_s), the energy gap between the bottom of the conduction band and top of the valence band (E_g), the total value of magnetism (M), and binding energy (E_b) of HS-G/MoS_2 and C sites vacancy defects in HS-G/MoS_2 materials.

HS-G/MoS_2 and C sites vacancy defects in HS-G/MoS_2 materials	E_f (eV)	E_s (eV)	E_g (eV)	M (μ_B/cell)	E_b (eV)
HS-G/MoS_2	0.32	—	—	0.00	0.25
R-1C vacancy defects in HS-G/MoS_2	0.52	0.20	0.15	−0.75	0.24
L-1C vacancy defects in HS-G/MoS_2	0.53	0.21	0.13	−0.75	0.24
C-1C vacancy defects in HS-G/MoS_2	0.54	0.22	0.14	−0.12	0.24
2C vacancy defects in HS-G/MoS_2	0.56	0.24	0.37	+0.39	0.23

total energy of a supercell with the defects, n_C *is* the numbers of C atoms removed from the perfect supercell to introduce a vacancy, μ_C is chemical potentials of C atoms, and E_T *(perfect)* is the total energy of the neutral perfect supercell, respectively. Figures 1(d)–1(f) are interlayer and interatomic distances measurement geometries of HS-G/MoS_2, 1C, and 2C atom vacancy defects in HS-G/MoS_2 geometries, respectively.

We have analyzed the structural properties of HS-G/MoS_2 and C sites vacancy defects in HS-G/MoS_2 materials and then obtained the data of interlayer distances which are given in Table 2. Also, interatomic distances of HS-G/MoS_2 and its C sites vacancy defects in HS-G/MoS_2 materials are given in SI (Table S1).

From Table 2, we found that HS-G/MoS_2 geometry is more compressed than C sites vacancy defects in HS-G/MoS_2 geometries, and compactness of material increases with a decrease in its defects concentrations. Also, we found that the C-1C vacancy defects structure is slightly compact than other R-1C and L-1C vacancy defects structures.

3.2. Electronic and Magnetic Properties. To know the electronic and magnetic properties of HS-G/MoS_2 and C sites vacancy defects in HS-G/MoS_2 materials, we first consider the key characteristics of freestanding Graphene supercell, monolayer MoS_2 supercell, and G/MoS_2 heterostructure. From band structure calculations, Graphene has zero bandgap energy because the states below the Fermi level characterized by π bonds and states above the Fermi level characterized by π^* antibonding states and corresponding bands meet at Fermi level that is Dirac cone. The monolayer MoS_2 is an intrinsic semiconductor with a direct band of value 1.65 eV; this value is close to the experimentally reported value of 1.80 eV [10, 33]. The zero-bandgap energy material (Graphene) and wide-bandgap energy material (MoS_2) are joined together to form vdWs HS-G/MoS_2 material with 4.13% of the lattice mismatch as shown in Figure 1(c). In HS-G/MoS_2, n-type Schottky contact is formed with a Schottky barrier height of 0.56 eV as shown in Figure 3(a). Figure 3(a) represents the band structure plot of HS-G/MoS_2, where the x-axis represents high symmetric points in the first Brillouin zone and the y-axis represents the corresponding energy values. We have taken 100 k-points along the specific direction of the irreducible Brillouin zone to get a fine band structure by choosing Γ-M-K-Γ high

Table 2: The interlayer distances of (i) HS-G/MoS_2 and (ii) C sites vacancy defects in HS-G/MoS_2 materials.

	Interlayer distances of HS-G/MoS_2 along x-, y-, and z-axis			Interlayer distances of C sites vacancy defects in HS-G/MoS_2 materials along x-, y-, and z-axis											
				C-Mo				C-US				C-DS			
	C-Mo	C-US	C-DS	2C	C-1C	R-1C	L-1C	2C	C-1C	R-1C	L-1C	2C	C-1C	R-1C	L-1C
x-axis (Å)	0.29	1.88	0.89	0.30	0.29	0.29	0.29	1.89	1.87	1.88	1.88	0.90	0.89	0.89	0.89
y-axis (Å)	0.25	1.16	1.17	0.28	0.26	0.26	0.27	1.18	1.17	1.17	1.18	1.18	1.16	1.16	1.17
z-axis (Å)	5.88	4.34	7.47	5.92	5.90	5.91	5.91	4.38	4.36	4.36	4.37	7.50	7.48	7.49	7.49

Here, (C-Mo), (C-US), and (C-DS) represent distance from C atom in Graphene to Mo atom in MoS_2, distance from C atom in Graphene to upper S atom in MoS_2, and distance from C atom in Graphene to down S atom in MoS_2, respectively.

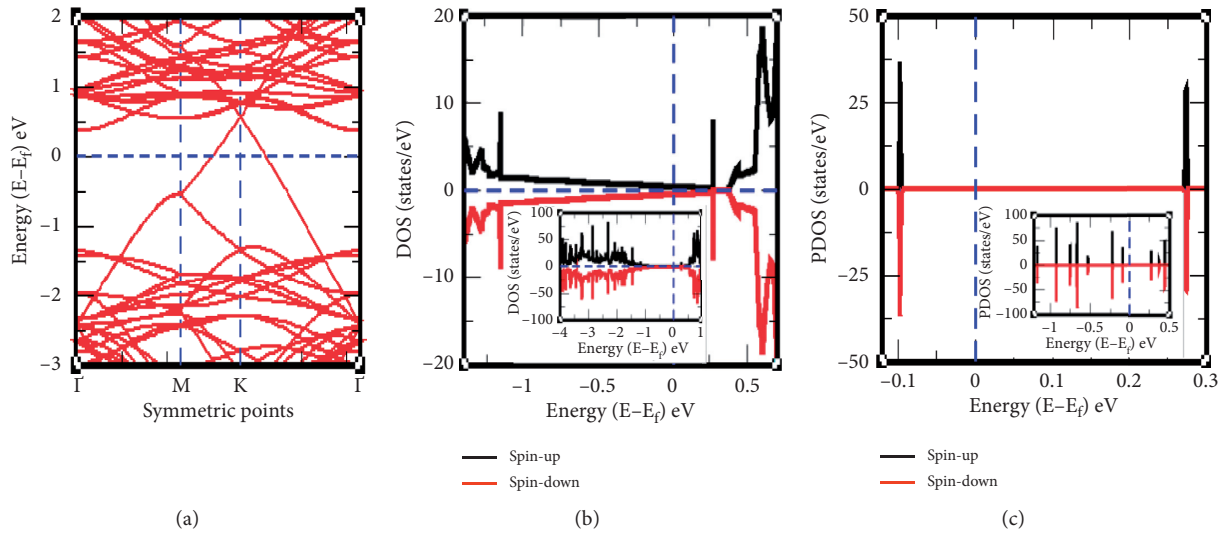

Figure 3: (a) Band structure of HS-G/MoS_2, where horizontal dotted line represents the Fermi level. (b) Spin-up and spin-down electrons are symmetrically distributed in the DOS plot of HS-G/MoS_2. (c) Spin-up and spin-down electrons are symmetrically distributed in the PDOS plot of HS-G/MoS_2. In all DOS and PDOS plots, the vertical dotted line represents the Fermi level. States above the horizontal dotted line represent spin-up electrons and states below the horizontal dotted line represents spin-down electrons.

symmetric points. We found that the Dirac point shifted 0.56 eV above the Fermi level in HS-G/MoS_2, which shows that HS-G/MoS_2 is metallic in nature. The shift in the Dirac point is in good agreement with the previously reported value of 0.49 eV [10, 35]. The Dirac point is formed at 0.56 eV height from the Fermi level in HS-G/MoS_2, because higher values of potential barrier existed between the positions of C and S atoms in Graphene and monolayer MoS_2 surfaces separately. The work function value of HS-G/MoS_2 is greater than MoS_2; as a result, electrons are moved from Graphene to MoS_2 surface making n-type Schottky contact [5, 36]. Figures 3(b) and 3(c) represent the density of states (DOS) and partial density of states (PDOS) plots of HS-G/MoS_2, where the y-axis represents spin-up and spin-down electrons states of DOS/PDOS and the x-axis represents the corresponding energy values.

In addition, to tune the electronic properties at C sites vacancy defects in HS-G/MoS_2 materials, we used band structure calculations of R-1C, L-1C, C-1C, and 2C atom vacancy defects in HS-G/MoS_2 materials as shown in Figure 4, where the x-axis represents high symmetric points in the first Brillouin zone and the y-axis represents the corresponding energy values. We have also taken 100 k-points along the specific direction of the irreducible Brillouin zone by choosing Γ-M-K-Γ high symmetric points.

We found that the Dirac point is not formed in electronic band structures and a small energy gap formed between the lower energy level of the conduction band and upper energy level of the valence band in R-1C, L-1C, C-1C, and 2C atom vacancy defects in HS-G/MoS_2 materials. These R-1C, L-1C, C-1C, and 2C vacancy defects materials have opened narrow bandgap of values 0.15 eV, 0.13 eV, 0.14 eV, and 0.37 eV, respectively. Thus, the strength of metallic nature decreased with an increase in the concentration of defects. It is obvious that electronic configurations of valence electrons in C, Mo, and S atoms are [He] $2s^2\ 2p^2$, [Kr] $4\,d^5\ 5s^1$, and [Ne] $3s^2\ 3p^4$, respectively. Each C atom has a single spin-up in $2p_x$ and $2p_y$ and vacancy in $2p_z$ suborbital; Mo atom has one unpaired spin-up in suborbital 5s and $4d_{xy}$, $4d_{xz}$, $4d_{yz}$, $4d_x^2$-$_y^2$, and $4d_z^2$; S atom has paired spins (up and down) in $3p_x$ suborbital and one unpaired spin-up in $3p_y$ and $3p_z$ suborbital. We have prepared a stable structure of 2C atom vacancy defects in HS-G/MoS_2 materials by removing two C atoms

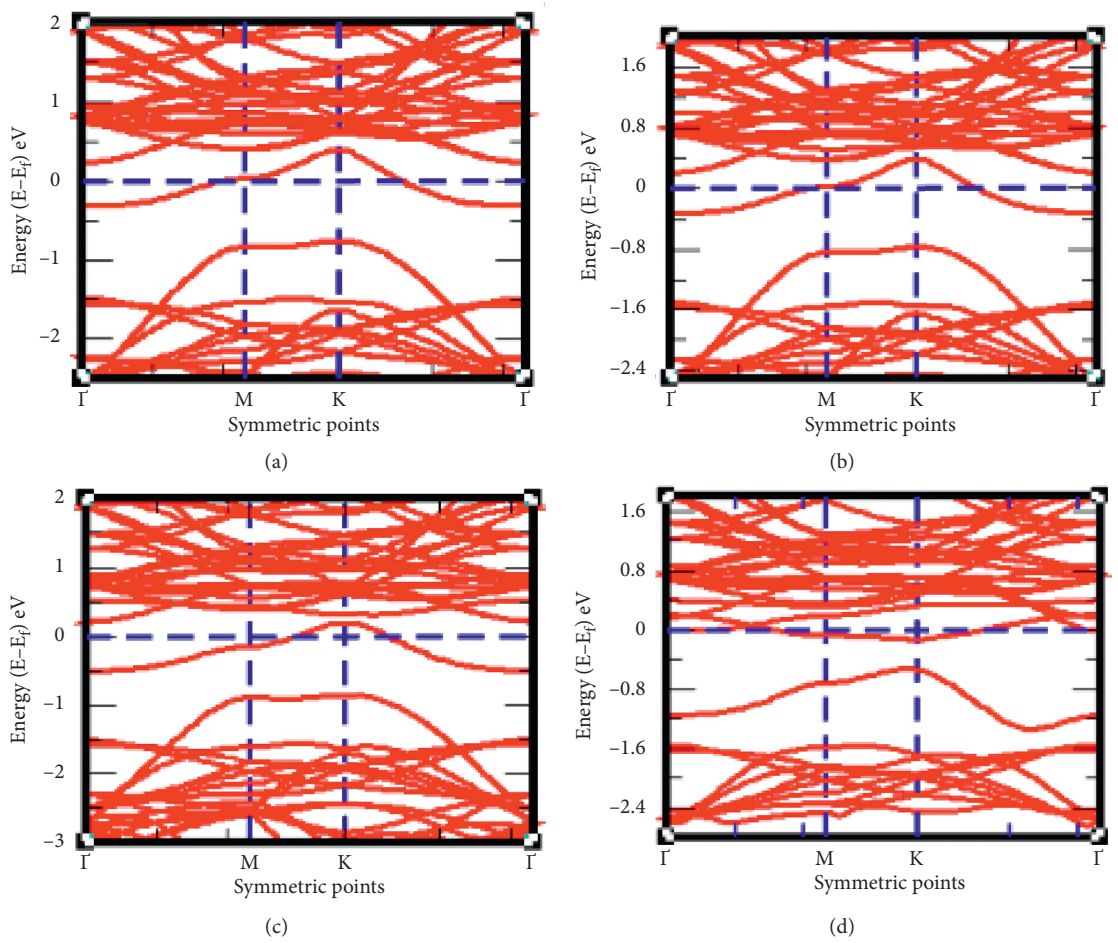

Figure 4: (a) Band structure of R-1C atom vacancy defects in HS-G/MoS_2, (b) band structure of L-1C atom vacancy defects in HS-G/MoS_2, (c) band structure of C-1C atom vacancy defects in HS-G/MoS_2, and (d) band structure of 2C atom vacancy defects in HS-G/MoS_2, where the horizontal dotted line represents Fermi level.

together from HS-G/MoS_2 material containing 59 atoms, as shown in Figure 2(d). Similarly, R-1C, L-1C, and C-1C atom vacancy defects in HS-G/MoS_2 stable materials are prepared by pulling out right 1C, left 1C, and centre 1C positions of carbon atoms from HS-G/MoS_2 structure having 59 atoms, respectively, as shown in Figures 2(a)–2(c). These vacancy positions of carbon atoms developed unpaired spin electrons in suborbital of atoms of 2C defects in HS-G/MoS_2 structure. Similarly, carbon atom vacancy in R-1C, L-1C, and C-1C defects in HS-G/MoS_2 materials produced unpaired spin electrons in the suborbital of atoms. Due to the unpaired total spin-up and total spin-down electrons in the orbitals of atoms in the system, unequal Fermi energy values are obtained in HS-G/MoS_2 and its C sites vacancy defect materials. Therefore, we found that the Fermi energy of HS-G/MoS_2 material has value 0.32 eV and R-1C, L-1C, C-1C, and 2C atom vacancy defects in HS-G/MoS_2 materials have values 0.52 eV, 0.53 eV, 0.54 eV, and 0.56 eV, respectively. It means that the Fermi level shifted upwards (towards conduction band) by 0.20 eV, 0.21 eV, 0.22 eV, and 0.24 eV values, respectively, which means Schottky barrier transition from p-type to n-type Schottky contact by the movement of interfacial charges [35]. The formation of n-type Schottky contact can provide important information for enhancing the power given by high efficiency Schottky nanoelectronic devices [37]. The parameters of Fermi level shift and energy gap look to be associated with each other. Also, they are increased with an increase in its vacancy defects concentrations in materials as shown in Table 1.

To get well competency of electronic and magnetic properties of materials, we have carried out DOS and PDOS calculations [23]. Figures 5(a)–5(d) represent DOS plots of R-1C, L-1C, C-1C, and 2C atom vacancy defects in HS-G/MoS_2 materials, respectively, and Figures 6(a)–6(d) represent PDOS plots of R-1C, L-1C, C-1C, and 2C atom vacancy defects in HS-G/MoS_2 materials, respectively, where the vertical dotted line represents Fermi energy level and the horizontal line separates states of spin-up and spin-down electrons in the orbitals of C, Mo, and S atoms; i.e., the states above the horizontal line represent spin-up electrons and a state below the horizontal line represents spin-down electrons.

The magnetic properties of materials can be investigated by the analysis of spins of electrons distributed in DOS and PDOS plots. The asymmetrically distributed spin-up and spin-down of atoms in DOS and PDOS plots mean that

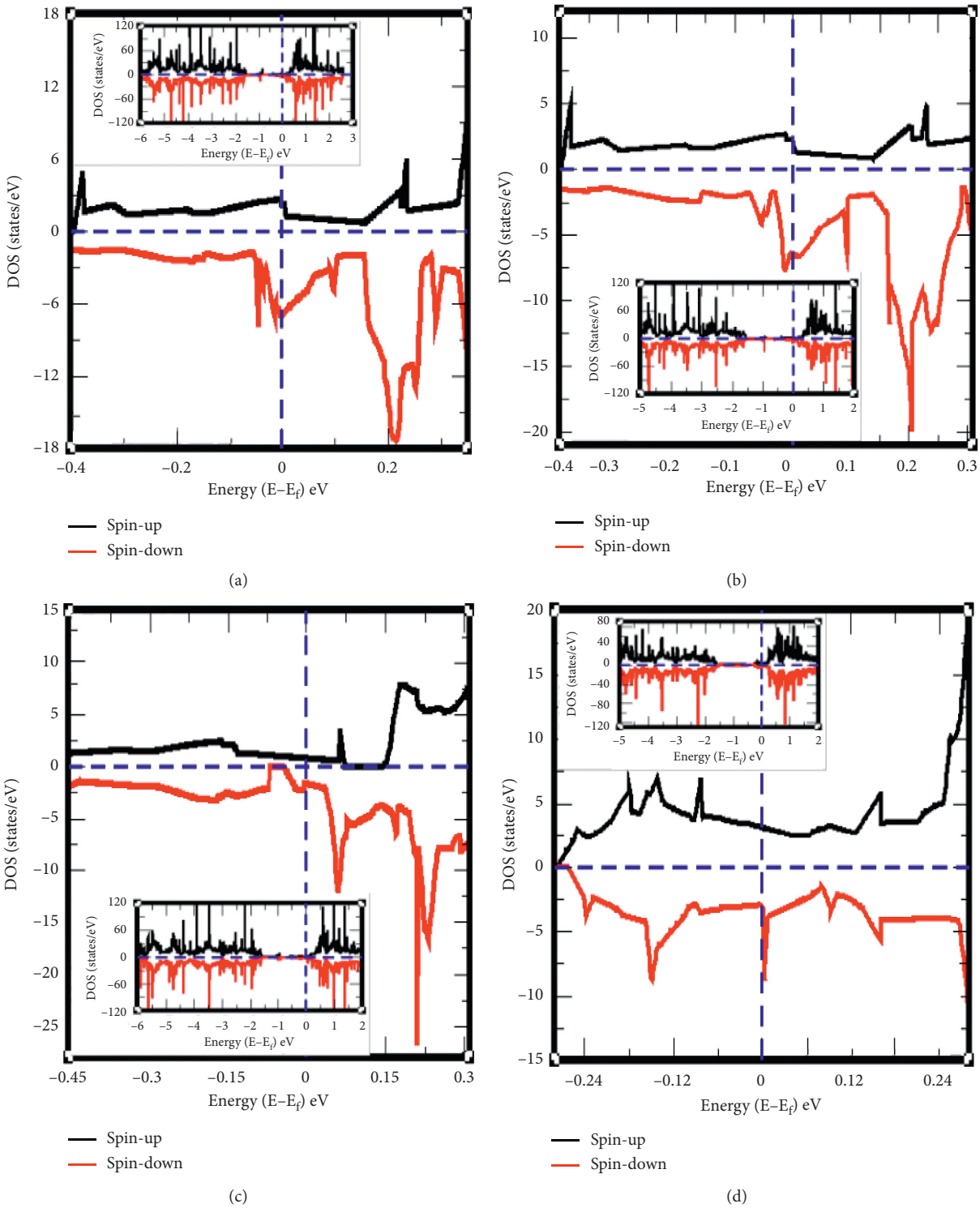

Figure 5: DOS plot of up and down states of spin electrons in the orbitals of C, Mo, and S atoms in (a) R-1C vacancy defects in HS-G/MoS_2 material, (b) L-1C vacancy defects in HS-G/MoS_2 material, (c) C-1C vacancy defects in HS-G/MoS_2 material, and (d) 2C vacancy defects in HS-G/MoS_2 material, where the states above the horizontal dotted line represent spin-up electrons and a state below the horizontal dotted line represents spin-down electrons.

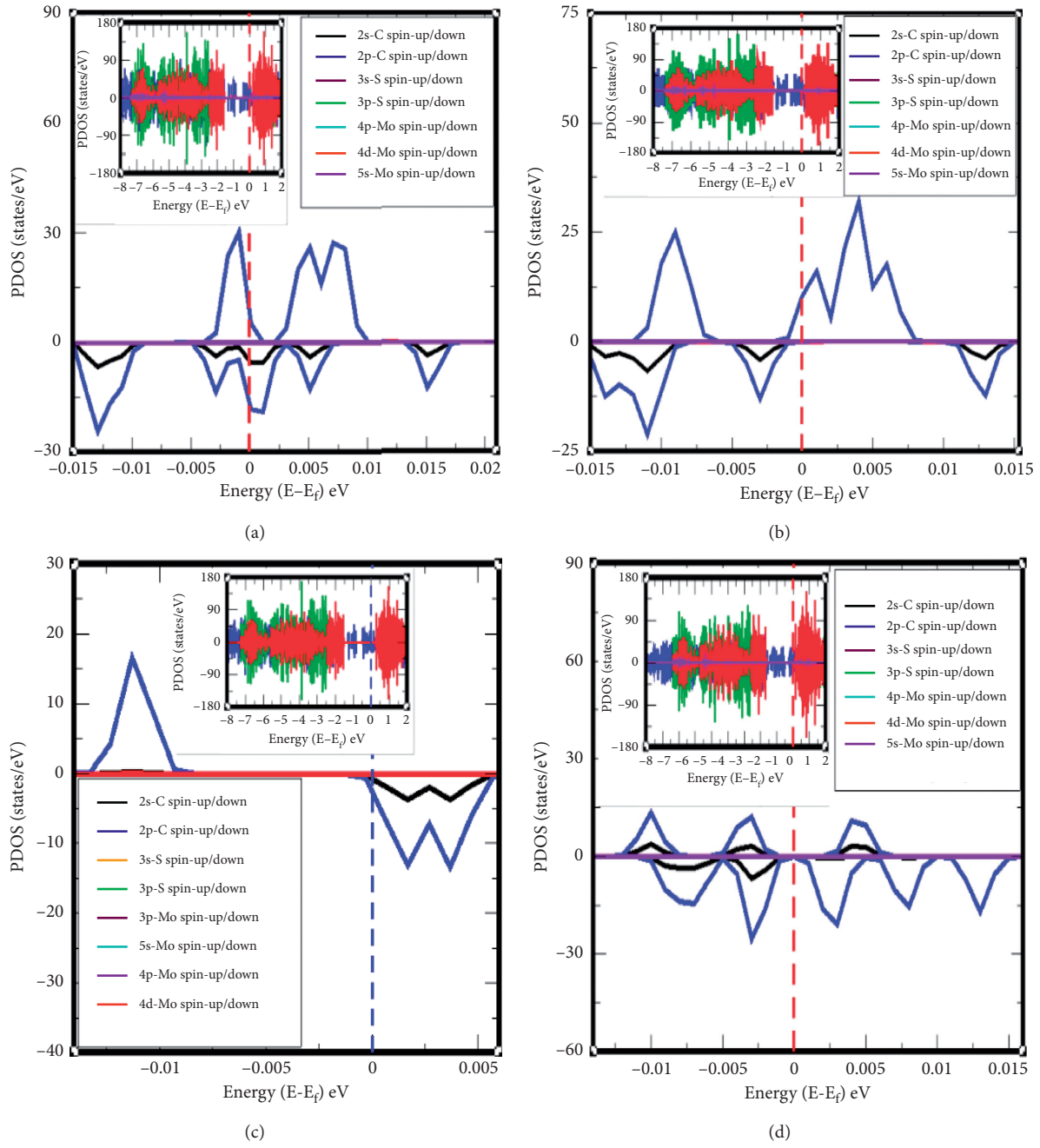

Figure 6: (a) PDOS plot of individual spin-up and spin-down electrons orbital of all atoms in R-1C atom vacancy defects in HS-G/MoS_2. (b) PDOS plot of individual spin-up and spin-down electrons orbital of all atoms in L-1C atom vacancy defects in HS-G/MoS_2. (c) PDOS plot of individual spin-up and spin-down electrons orbital of all atoms in C-1C atom vacancy defects in HS-G/MoS_2. (d) PDOS plot of individual spin-up and spin-down electrons orbital of all atoms in 2C atom vacancy defects in HS-G/MoS_2, where the states above the horizontal line represent spin-up electrons and a state below the horizontal line represents spin-down electrons.

materials have magnetic properties. Similarly, symmetrically distributed spin-up and spin-down of atoms in DOS and PDOS plots mean that materials carry nonmagnetic properties. We observed the spin-up and spin-down states of electrons, which are symmetrically distributed in the DOS and PDOS plot of HS-G/MoS_2 material as shown in Figures 3(b) and 3(c). Hence, HS-G/MoS_2 is a nonmagnetic material.

In addition, we have done the DOS and PDOS analysis of R-1C, L-1C, C-1C, and 2C atom vacancy defects in HS-G/MoS_2 materials. The data of magnetic moment calculations of these materials are given in SI (Table S2). The PDOS plots of 2s and 2p orbital of C atoms, 4p, 4d, and 5s orbital of Mo atoms, and 3s and 3p orbitals of S atoms in R-1C atom vacancy defects in HS-G/MoS_2 material are shown in Figure 6(a). PDOS value near the Fermi level of 2s and 2p orbitals of C atoms reflects that spin-up and spin-down states are asymmetrical. We found that the total magnetic moment of R-1C in HS-G/MoS_2 has a value −0.75 μ_B/cell;

this is due to 2s and 2p spins electrons in the orbitals of C atoms. Also, the magnetic moment given by spins of electrons in 2s and 2p orbitals of C atoms is separately calculated, which have −0.24 $\mu_{B/}$cell and −0.51 $\mu_{B/}$cell values, respectively. These values are obtained by calculating the net magnetic moment given by spin-up and spin-down electrons of carbon atoms in the structure. The negative values of magnetic moment reveal that spin-down electrons of atoms have a principal role compared to spin-up electrons of atoms for magnetism in the system. This means that other atoms do not play a role in the magnetism of R-1C atom vacancy defects in HS-G/MoS_2. In Figure 6(b), the unoccupied spin-up electron states in the 2p orbital of C atoms and spin-down electron states in the 2s and 2p orbital of C atoms are asymmetrically distributed near the Fermi level. Magnetic moment values given by 2s and 2p orbital of C atoms are $-0.23\mu_B$/cell and $-0.52\mu_B$/cell, respectively. Therefore, the total value of the magnetic moment of L-1C vacancy defects in HS-G/MoS_2 material is $-0.75\mu_B$/cell, due to dominant contributions of spin electrons in 2s and 2p orbital of C atoms in the system. Similarly, in Figure 6(c), the only unoccupied spin-down electron states are seen near the Fermi level, which reflects that spin states are asymmetrical. We have evaluated PDOS of C-1C defects in HS-G/MoS_2 material and found that the values of the magnetic moment due to spin electrons in 2s and 2p orbital of C atoms are $-0.07\mu_B$/cell & $-0.05\mu_B$/cell, respectively. Therefore, the total value of the magnetic moment given by spin electrons in the orbital of C atoms in the system is $-0.12\mu_B$/cell. In Figure 6(d), we saw that the asymmetrically distributed spin-up and spin-down electron states are presented beyond −0.0025 eV energy in the valence band and above 0.0024 eV energy in the conduction band. The magnetic moment given by 2s and 2p orbital of C atoms in the system has values $0.7\mu_B$/cell and $0.31\mu_B$/cell, respectively. These values are obtained by calculating net magnetism given by spin-up and spin-own electrons of atoms existing in the system. Therefore, the total value of the magnetic moment of 2C atom vacancy defects in HS-G/MoS_2 material is $+0.39\mu_B$/cell. The positive value of magnetic moment means that spin-up electrons of atoms have a preeminent role compared to spin-down electrons of atoms in the magnetism. In all these cases, 2s and 2p orbitals of C atoms have major contributions of magnetic moments in C sites vacancy defects in HS-G/MoS_2 materials, which are also shown in SI (Figure S1).

4. Conclusions

We have constructed HS-G/MoS_2 and C sites vacancy defects in HS-G/MoS_2 structures and investigated their structural, electronic, and magnetic properties by first-principle calculations with van der Waals corrections in the DFT-D2 levels of approximation. We studied structures of HS-G/MoS_2 and C sites vacancy defects in HS-G/MoS_2 materials and found that the nondefects structure is more compressed than defects structures. The binding energy of these materials is decreased with an increase in its defects concentrations. Then, we investigated the electronic and magnetic properties of these materials from the band structure calculations and DOS/PDOS analysis. From band structure calculations of HS-G/MoS_2, we found that it is metallic in nature. R-1C, L-1C, C-1C, and 2C atom vacancy defects in HS-G/MoS_2 materials have small energy gap of values 0.15 eV, 0.13 eV, 0.14 eV, and 0.37 eV, respectively. Thus, the strength of metallic nature decreased with an increase in the concentration of vacancy in structures. Also, we have calculated the Fermi energy level of pure and vacancy defects geometries, which shows that n-type Schottky barrier contact is formed due to the interfacial charge transfer. For better comprehension of the electronic and magnetic properties of materials, we have performed the DOS and PDOS calculations. We found that DOS and PDOS states of spin-up and spin-down electrons are symmetrically distributed in HS-G/MoS_2 and asymmetrically distributed in C sites vacancy defects in HS-G/MoS_2 materials. Therefore, HS-G/MoS_2 is a nonmagnetic material but C sites vacancy defects in HS-G/MoS_2 materials carry magnetic properties. The total magnetic moment in R-1C, L-1C, C-1C, and 2C atom vacancy defects in HS-G/MoS_2 materials is found to be $-0.75\mu_B$/cell, $-0.75\mu_B$/cell, $-0.12\mu_B$/cell, and $+0.39\mu_B$/cell, respectively. The spins of electrons in 2s and 2p orbitals of C atoms have the main role to bring a magnetic moment in all these materials. The strength of magnetic properties is developed in C sites vacancy defects in HS-G/MoS_2 materials due to the convenient arrangement of spin electrons in the structures.

Data Availability

The data used to support the findings of this study are available from the corresponding author upon request.

Conflicts of Interest

The authors declare that they have no conflicts of interest.

Acknowledgments

HKN acknowledges the UGC Nepal Award no. PhD-75/76-S&T-09 and network project NT-14 of ICTP/OEA. NPA acknowledges UGC Nepal (Grant CRG 073/74 -S&T -01).

Supplementary Materials

Table S_1: the interatomic distances measurement of HS-G/MoS_2 and C sites vacancy defects in HS-G/MoS_2 geometries, where (S-S), (Mo-Mo), and (C-C), respectively, represent the interatomic distance between two sulpher atoms in MoS_2, two molybdenum atoms, and two carbon atoms in Graphene. Table S_2: magnetic values generated by total and individual spin-up and spin-down electron orbital of C, Mo, and S atoms in pure and C sites vacancy defects (HS) in G/MoS_2 geometries from PDOS analysis. Figure S_1: (a) PDOS plot of total spin-up and spin-down electron orbital of all atoms in R-1C atom vacancy defects in HS-G/MoS_2. (b) PDOS plot of total spin-up and spin-down electron orbital of all atoms in L-1C atom vacancy defects in HS-G/MoS_2. (c) PDOS plot of total spin-up and spin-down

electron orbital of all atoms in C-1C atom vacancy defects in HS-G/MoS_2. (d) PDOS plot of total spin-up and spin-down electron orbital of all atoms in 2C atom vacancy defects in HS-G/MoS_2, where the states above the horizontal line represent spin-up electrons and a state below the horizontal line represents spin-down electrons. (*Supplementary Materials*)

References

[1] K. S. Novoselov, A. K. Geim, S. V. Morozov et al., "Electric field effect in atomically thin carbon films," *Science*, vol. 306, no. 5696, pp. 666–669, 2004.

[2] K. S. Novoselov, A. K. Geim, S. V. Morozov et al., "Two-dimensional gas of massless dirac fermions in graphene," *Nature*, vol. 438, no. 7065, pp. 197–200, 2005.

[3] E. V. Castro, K. S. Novoselov, S. V. Morozov et al., "Biased bilayer graphene: semiconductor with a gap tunable by the electric field effect," *Physical Review Letters*, vol. 99, no. 21, p. 216802, 2007.

[4] C. V. Nguyen and N. N. Hieu, "Effect of biaxial strain and external electric field on electronic properties of MoS_2 monolayer: a first-principle study," *Chemical Physics*, vol. 468, pp. 9–14, 2016.

[5] K. F. Mak, C. Lee, J. Hone, J. Shan, and T. F. Heinz, "Atomically thin MoS_2: a new direct-gap semiconductor," *Physical Review Letters*, vol. 105, no. 13, p. 136805, 2010.

[6] E. S. Kadantsev and P. Hawrylak, "Electronic structure of a single MoS_2 monolayer," *Solid State Communications*, vol. 152, no. 10, pp. 909–913, 2012.

[7] B. Radisavljevic, M. B. Whitwick, and A. Kis, "Small-signal amplifier based on single-layer MoS_2," *Applied Physics Letters*, vol. 101, no. 4, p. 043103, 2012.

[8] Y. Hu, M. Ruan, Z. Guo et al., "Structured epitaxial graphene: growth and properties," *Journal of Physics D: Applied Physics*, vol. 45, no. 15, p. 154010, 2012.

[9] C. V. Nguyen, "Tuning the electronic properties and Schottky barrier height of the vertical graphene/MoS_2 heterostructure by an electric gating," *Superlattices and Microstructures*, vol. 116, pp. 79–87, 2018.

[10] H. V. Phuc, N. N. Hieu, B. D. Hoi, L. T. T. Phuong, and C. V. Nguyen, "First principle study on the electronic properties and Schottky contact of graphene adsorbed on MoS_2 monolayer under applied out-plane strain," *Surface Science*, vol. 668, pp. 23–28, 2018.

[11] H. U. Din, M. Idrees, A. Albar et al., "Rashba spin splitting and photocatalytic properties of GeC–MSSe (M=Mo, W) van der Waals heterostructures," *Physical Review B*, vol. 100, no. 16, p. 165425, 2019.

[12] T. V. Vu, N. V. Hieu, H. V. Phuc et al., "Graphene/WSeTe van der Waals heterostructure: controllable electronic properties and Schottky barrier via interlayer coupling and electric field," *Applied Surface Science*, vol. 507, p. 145036, 2020.

[13] C. V. Nguyen, M. Idrees, H. V. Phuc et al., "Interlayer coupling and electric field controllable Schottky barriers and contact types in graphene/PbI_2 heterostructures," *Physical Review B*, vol. 101, no. 23, p. 235419, 2020.

[14] J. Wang, F. Ma, W. Liang, and M. Sun, "Electrical properties and applications of graphene, hexagonal boron nitride (h-BN), and graphene/h-BN heterostructures," *Materials Today Physics*, vol. 2, pp. 6–34, 2017.

[15] M. Ghorbani-Asl, P. D. Bristowe, K. Koziol, T. Heine, and A. Kuc, "Effect of compression on the electronic, optical and transport properties of MoS_2/graphene-based junctions," *2D Materials*, vol. 3, no. 2, p. 025018, 2016.

[16] Y. Ma, Y. Dai, M. Guo, C. Niu, and B. Huang, "Graphene adhesion on MoS_2 monolayer: an ab initio study," *Nanoscale*, vol. 3, no. 9, pp. 3883–3887, 2011.

[17] A. D. Phan, N. A. Viet, N. A. Poklonski, L. M. Woods, and C. H. Le, "Interaction of a graphene sheet with a ferromagnetic metal plate," *Physical Review B*, vol. 86, no. 15, p. 155419, 2012.

[18] W. J. Yu, Z. Li, H. Zhou et al., "Vertically stacked multi-heterostructures of layered materials for logic transistors and complementary inverters," *Nature Materials*, vol. 12, no. 3, pp. 246–252, 2013.

[19] M. S. Choi, G. H. Lee, Y. J. Yu et al., "Controlled charge trapping by molybdenum disulphide and graphene in ultrathin heterostructured memory devices," *Nature Communications*, vol. 4, no. 1, pp. 1–7, 2013.

[20] K. Roy, M. Padmanabhan, S. Goswami et al., "Graphene-MoS_2 hybrid structures for multifunctional photoresponsive memory devices," *Nature Nanotechnology*, vol. 8, no. 11, pp. 826–830, 2013.

[21] L. Debbichi, O. Eriksson, and S. Lebègue, "Electronic structure of two-dimensional transition metal dichalcogenide bilayers from ab initio theory," *Physical Review B*, vol. 89, no. 20, p. 205311, 2014.

[22] H. K. Neupane and N. P. Adhikari, "Structure, electronic and magnetic properties of 2D Graphene-Molybdenum diSulphide (G-MoS_2) heterostructure (HS) with vacancy defects at Mo sites," *Computational Condensed Matter*, vol. 24, p. e00489, 2020.

[23] C. Kittel, P. McEuen, and P. McEuen, *Introduction to solid state Physics*, vol. 8, pp. 140–303, Wiley, New York, NY, USA, 1996.

[24] M. V. Makarova, Y. Akaishi, T. Ikarashi, K. S. Rao, S. Yoshimura, and H. Saito, "Alternating magnetic force microscopy: effect of Si doping on the temporal performance degradation of amorphous FeCoB magnetic tips," *Journal of Magnetism and Magnetic Materials*, vol. 471, pp. 209–214, 2019.

[25] H. X. Peng, F. Qin, and M. H. Phan, *Ferromagnetic Microwire Composites: From Sensors to Microwave Applications*, Springer, New York, NY, USA, 2016.

[26] P. Hohenberg and W. Kohn, "Inhomogeneous electron gas," *Physical Review*, vol. 136, no. 3B, p. B864, 1964.

[27] S. Grimme, "Accurate description of van der Waals complexes by density functional theory including empirical corrections," *Journal of Computational Chemistry*, vol. 25, no. 12, pp. 1463–1473, 2004.

[28] P. Giannozzi, S. Baroni, N. Bonini et al., "Quantum ESPRESSO: a modular and open-source software project for quantum simulations of materials," *Journal of Physics: Condensed Matter*, vol. 21, no. 39, p. 395502, 2009.

[29] J. P. Perdew, K. Burke, and M. Ernzerhof, "Generalized gradient approximation made simple," *Physical Review Letters*, vol. 77, no. 18, p. 3865, 1996.

[30] B. G. Pfrommer, M. Côté, S. G. Louie, and M. L. Cohen, "Relaxation of crystals with the quasi-Newton method," *Journal of Computational Physics*, vol. 131, no. 1, pp. 233–240, 1997.

[31] R. M. Martin and R. M. Martin, *Electronic Structure: Basic Theory and Practical Methods*, Cambridge University Press, Cambridge, UK, 2004.

[32] N. Marzari, D. Vanderbilt, A. De Vita, and M. C. Payne, "Thermal contraction and disordering of the Al(110) surface," *Physical Review Letters*, vol. 82, no. 16, p. 3296, 1999.

[33] S. Ahmad and S. Mukherjee, "A comparative study of electronic properties of bulk MoS_2 and its monolayer using DFT technique: application of mechanical strain on MoS_2 monolayer," *Graphene*, vol. 3, no. 4, pp. 52–59, 2014.

[34] Z. Hou, X. Wang, T. Ikeda et al., "Interplay between nitrogen dopants and native point defects in graphene," *Physical Review B*, vol. 85, no. 16, p. 165439, 2012.

[35] B. Liu, L.-J. Wu, Y.-Q. Zhao, L.-Z. Wang, and M.-Q. Cai, "First-principles investigation of the Schottky contact for the two-dimensional MoS_2 and graphene heterostructure," *RSC Advances*, vol. 6, no. 65, pp. 60271–60276, 2016.

[36] N. N. Hieu, H. V. Phuc, V. V. Ilyasov et al., "First-principles study of the structural and electronic properties of graphene/MoS2 interfaces," *Journal of Applied Physics*, vol. 122, no. 10, p. 104301, 2017.

[37] K. D. Pham, N. N. Hieu, H. V. Phuc et al., "Layered graphene/GaS van der Waals heterostructure: controlling the electronic properties and Schottky barrier by vertical strain," *Applied Physics Letters*, vol. 113, no. 17, p. 171605, 2018.